International Journal of Engineering & Technology, 7 (4.13) (2018) 195-201

International Journal of Engineering & Technology

Website: www.sciencepubco.com/index.php/IJET

Research paper

Nonlinear reduced order model of high aspect ratio rectangular wing plate

Thinesh C, M Y Harmin*

Department of Aerospace Engineering, Faculty of Engineering, Universiti Putra Malaysia, 43400 Serdang, Selangor, Malaysia
**Corresponding author E-mail: myazdi@upm.edu.my*

Abstract

This paper presents a Combined Modal Finite Element (CMFE) approach to develop a Nonlinear Reduced Order Model (NROM) in order to characterize the nonlinear properties of the wing plate model. The wing plate model is subjected to three types of loading cases. The first case considers a uniformly distributed loading on the whole wing plate model for describing the bending deflection; the second case considers a uniformly distributed loading on both leading and trailing edges with one of them of an opposite direction for describing the twisting deflection; the third case considers the loading on the leading edge for describing a combination of bending-twisting deflection. The accuracy of the results is represented in the form of mean error, the standard deviation of the error and the percentage of error. From the findings, the NROMs are able to predict the nonlinear deformations of the wing plate with a minimal computational time and reasonably good accuracy. The results also indicate the importance of the selection modes when conducting the analysis.

Keywords: *high aspect ratio wing; nonlinear; reduced order model; regression analysis.*

1. Introduction

Nowadays, current aircraft designs are mostly of high aspect ratio (HAR) and flexible wings, which are not limited to civil aircraft but unmanned aerial vehicles as well. Although better aerodynamic efficiency can be gained with such characteristics of the wing, it is easily exposed to large deformations as high as 30% of the wing semi span even at a relatively low aerodynamic loading [1,2]. This causes the overall stiffness of the wing to behave in the nonlinear manner [3-5]. This behaviour is mainly due to either the geometric stiffening or softening, causing the conventional linear aeroelastic analysis to be infeasible under these conditions [3-6]. One of the infamous incidents that highlights the impracticability of the aeroelastic analysis is the NASA Helios mishap, which the main cause of the incident is later found to be the lack of appropriate analyses for highly flexible aerospace structures [7,8].

Patil *et al.* [9] have highlighted significant changes that occur in the natural frequency of the structural model, which lead to the decrement of flutter velocity due to the nonlinear coupling of edgewise bending and torsional modes. That research has also conveyed the effect of nonlinearity on the trim solution. It has also portrayed the importance of inclusion of nonlinearity in the analysis in order to predict the actual deformation. In other work, Palacios *et al.* [10] have investigated the parameters affected due to geometric nonlinearity, which is inclusive of gust response, longitudinal stability and body-free flutter. The work has concluded with a highlight on the necessity of a tool to predict the nonlinearity parameters of the wing in order to estimate the aeroelastic characteristics in nonlinear region with significant time reduction to improve computational efficiency of the analysis. McEwan *et al.* [11] have used a combined modal finite element (CMFE) approach to model the geometrically nonlinear panels used for the analysis. A comparison has been conducted between CMFE approach and direct integration of finite element method (FEM). For this approach, a number of load cases has been pre-determined and static analysis is conducted to extract the displacements of the panels due to the loads. The displacements are then curve-fitted using a regression analysis to predict the nonlinear stiffness coefficients. The results of the study have indicated good agreement between CMFE and FEM results, and also have shown to reduce the computational time of the analysis significantly.

Harmin *et al.* [6] proposed to implement the CMFE approach on the High Altitude Long Endurance (HALE) wing model by Patil and Hodges [9]. The motive of the study was to predict the static deflection, gust response and limit cycle oscillations (LCO) behaviour of the wing when subjected to the geometric nonlinearity. The CMFE was coupled together with rational function approximation of the doublet lattice aerodynamics using Roger Method, hence enabling the static aeroelastic and gust analyses to be performed with the inclusions of the geometric nonlinearity.

In this study, CMFE [6,11] approach is utilized to describe the nonlinear properties of the wing plate model under three types of distributed loading. The linear and nonlinear static analyses are conducted for a range of test cases. Once the nonlinear reduced order model (NROM) is developed, it is validated with the corresponding nonlinear finite element solutions.

2. Methodology

2.1. Wing plate model

Figure 1 portrays the wing plate simulation model utilized in this study. Note that a fully clamped boundary condition is defined at one end of the wing plate model as shown in Figure 1(b). Properties of the wing plate model are summarized in Table 1.

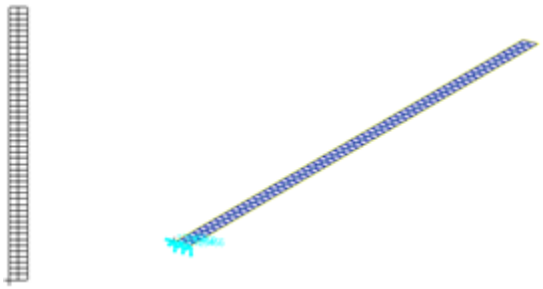

(a) **(b)**

Fig. 1: (a) Wing plate model meshing; (b) Wing plate model with defined boundary conditions

Table 1: Parameters of the wing plate model

Parameter	Value
Span, b	0.8 m
Chord length, c	0.05 m
Density, ρ	7833.413 kg/m^3
Young's Modulus, E	206843 MPa
Poisson's Ratio, v	0.295

2.2. NROM via CMFE approach

The CMFE [6,11] approach allows the NROM to be characterized from a series of prescribed loading cases of the nonlinear static solution. The nonlinear stiffness terms are identified through curve fitting of the nonlinear force-displacement relationship using the ordinary polynomial approach and regression analysis. This term can then be added to the linear equation of motion in modal coordinate, which demonstrates the inclusion of geometric nonlinearities to the conventional modal space system. Prior to this, a normal mode analysis is to be conducted to obtain the eigensolution consisting the eigenvalue and its corresponding eigenvector solutions. Once the NROM is developed, it is then used to predict the deflection for a defined force input and the result is verified with the conventional FEA results of nonlinear static solutions. It should be noted that the linear static analysis has to be performed as well in order to observe the degree of nonlinearities of the wing plate model when compared to the nonlinear static solution.

Based on the mathematical modelling used by Harmin *et al.* [6,12], the static system equation is given by Eqn. 1, where $[\boldsymbol{E_L}]$ is diagonal matrices of size NR × NR; $\{\boldsymbol{F}\}$ is the NR × 1 applied modal force; $\{\boldsymbol{E_{NL}}(p)\}$ is a polynomial form as the product of Nth order modal displacements multiplied by the unknown nonlinear stiffness coefficients and p is the modal displacement.

$$[\boldsymbol{E_L}]\{p\} + \{\boldsymbol{E_{NL}}(p)\} = \{\boldsymbol{F}\} \quad (1)$$

From the static system equation, the left-hand side of the equation is the stiffness restoring forces which compromises of the linear and nonlinear stiffness. By rearranging Eqn. 1, Eqn. 2 can be obtained.

$$\{\boldsymbol{F}\} - [\boldsymbol{E_L}]\{p\} = \{\boldsymbol{E_{NL}}(p)\} \quad (2)$$

From the equations above, let:

$$[D] = [\{\boldsymbol{F}\} - [\boldsymbol{E_L}]\{p\}] \quad (3)$$

where D is 1 × NL vector; NL is the number of load cases considered for the investigation. Since $\{\boldsymbol{E_{NL}}(p)\}$ is a polynomial function hence the matrix is split into:

$$\{\boldsymbol{E_{NL}}(p)\} = [p^2 \quad p^3 \quad \cdots]\begin{bmatrix} A_1 \\ A_2 \\ \vdots \end{bmatrix} \quad (4)$$

where A_1 and A_2 are the constants in the polynomial equation. The polynomial constants can be found by:

$$\begin{bmatrix} A_1 \\ A_2 \\ \vdots \end{bmatrix} = [D]\,[p^2 \quad p^3 \quad \cdots]^{inv} \quad (5)$$

where $[p^2 \quad p^3 \quad \cdots]^{inv}$ is the pseudo-inverse of the $[p^2 \quad p^3 \quad \cdots]$ matrix. Once the polynomial constants are found, the NROM equations can then be formed. By defining the force to which is to be investigated, a Newton Raphson method analysis is employed on the NROM equation in order to find the modal displacement for the specified force.

The modal force can be obtained by Eqn. 6 while the physical displacement can be obtained by Eqn. 7.

$$\{\boldsymbol{F}\} = [\psi]^T\{\mathbb{F}\} \quad (6)$$

$$[x] = [\psi]^{inv}[p] \quad (7)$$

To verify the obtained results, the mean and standard deviation of the error for each analysis are calculated and displayed graphically; where the error is the differences between the solution obtained by NROM and FEA of the nonlinear static solution.

2.3. Types of load cases

The wing plate model is subjected to three types of load cases. The first case is of uniformly distributed loading over the whole wing plate model to describe a bending profile. The second case is uniformly distributed loading along the leading edge and trailing edge of the wing plate model with one of them in opposite direction to describe a twisted profile. Meanwhile, the third case is of uniformly distributed loading over the leading edge of the wing plate model, which constitutes both deformation profiles from the previous two cases. The test-cases are ensured to having both linear and nonlinear region of deformations has to be covered.

2.3.1. Case 1: Uniform loading

The entire wing plate model is subjected to a uniformly distributed loading, which is defined as nodal forces on each node specified on the wing plate structural model. The distribution of the forces in this case is portrayed in Figure 2. The tip deflections for the selected test-cases under linear and nonlinear circumstances are shown in Figure 3. From Figure 3, the importance of the study can be highlighted as there is a huge difference between the linear static and nonlinear static analysis results. It should be noted that the selected test-cases are ensured to cover both linear and nonlinear region. The main reason for the selection criteria of the test-cases to be ranging from the linear to nonlinear region is for the NROM modal developed to be able to predict the linear deformation of the wing plate as well as the nonlinear deformation of it.

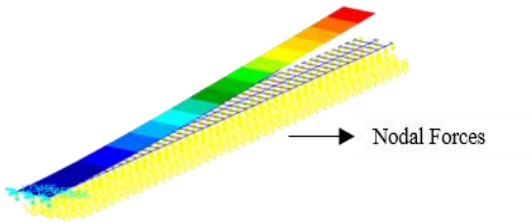

Fig. 2: Distribution of uniform loading on wing plate model

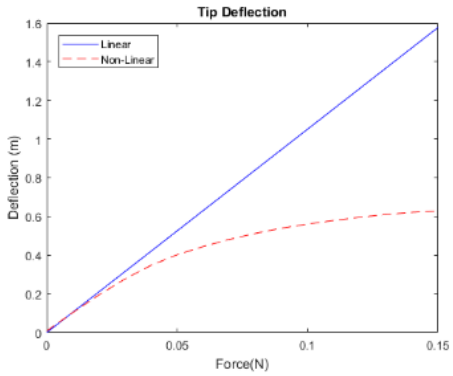

Fig. 3: Tip deflection for uniform loading

2.3.2. Case 2: Twist loading

The case, twist loading, is defined as combinations of forces to induce a twisting profile on the model it is subjected to. Hence, a leading edge and trailing edge of the wing plate model is subjected to uniformly distributed forces of equal magnitude but in opposite directions to induce a twisting profile of the wing plate model. Figure 4 shows the twist loading on the wing plate model. On the other hand, Figure 5 presents the tip deformations for the selected test-cases under linear and nonlinear circumstances. Similarly, the test-cases are selected to ensure both linear and nonlinear properties of the wing plate model are characterized.

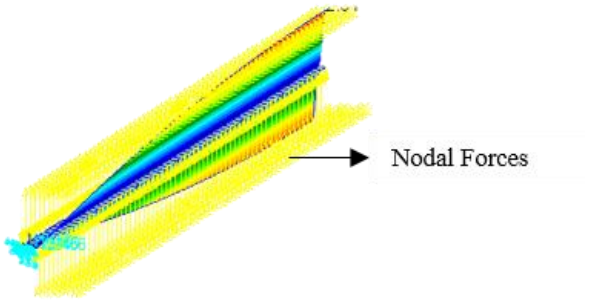

Fig. 4: Distribution of uniform loading on the leading edge and trailing edge of the wing model plate model

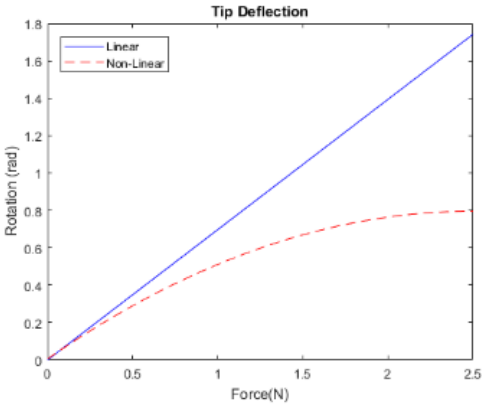

Fig. 5: Tip deformation for twist loading

2.3.3. Case 3: Leading edge loading

The wing plate model's leading is subjected to a uniform distributed loading which leads to a combination of twist and bending deformation. Figure 6 shows the leading edge loading subjected on the wing plate model. In the meantime, Figure 7 presents the tip deformations for the selected test-cases under linear and nonlinear circumstances on the leading and trailing edge as well as the rotation of the wing plate model.

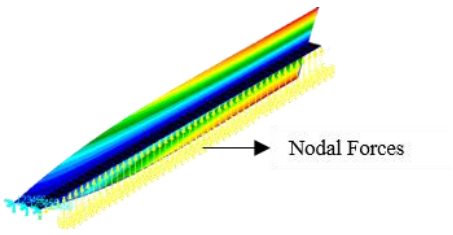

Fig. 6: Distribution of uniform loading on the leading edge of the wing model plate model

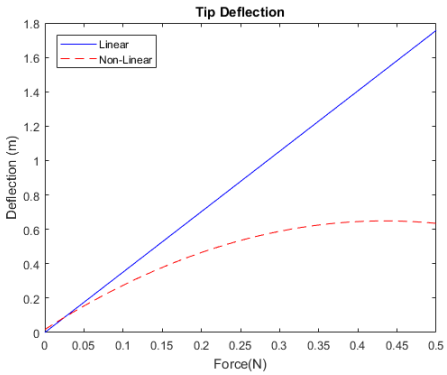

(a) Tip bending deflection at leading edge

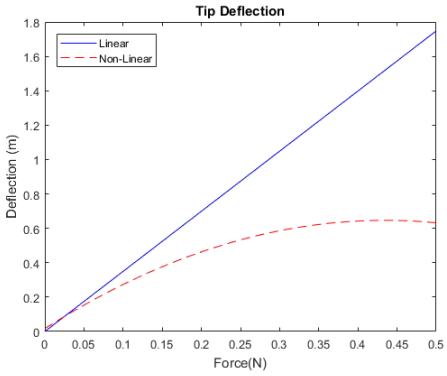

(b) Tip bending deflection at trailing edge

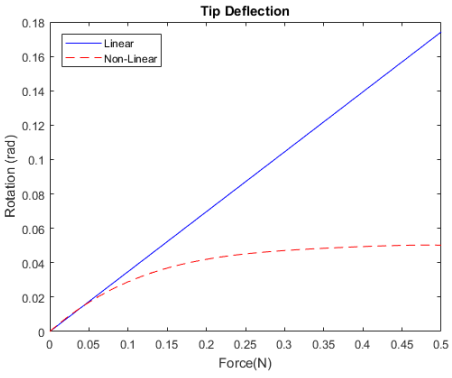

(c) Tip twisting deflection

Fig. 7: Tip deformation for bending and twisting deflections

3. Results and discussions

3.1. Investigation of NROM produced with Case 1 and Case 2 load cases to predict deformations due to Case 1, Case 2 and Case 3

The NROM equations of Case 1 and Case 3 load cases are summarized in Table 2.

Table 2: NROM equations

Case 1	$\boldsymbol{F_{B1}} = 153\ P_{B1} + (1.51 \times 10^{3})\ P_{B1}^{2} + (5.79 \times 10^{3})\ P_{B1}^{3}$
Case 2	$\boldsymbol{F_{T1}} = 146369\ P_{T1} + (4.84 \times 10^{7})\ P_{T1}^{2} + (6.63 \times 10^{9})\ P_{T1}^{3}$

3.1.1. NROM (Case-1, Case-2) for Case-1

Figure 8 presents the summary of mean error and standard deviation of the NROM analysis for the test cases. Based on Figure 8, it was found the NROM was unable to characterize the linear properties of the wing plate model effectively. This has been expected since the NROM equations formed are more centred on the nonlinear properties of the wing plate model. However, for the test-case with the lowest magnitude of force, the mean error was found to be of approximately 3.5 cm with a standard deviation of approximately 2.5 cm. However, for the other test-cases, the mean error and the standard deviation of the error is relatively lower in comparison to the test-case with the lowest magnitude of force. At extremely high deflections, the error of the NROM analysis increases, this is due to limitations of the equation to which the additional input of mode, test cases and increment in the order of the equation are possible solutions that can be opted to increase the accuracy of the analysis for higher deflection ranges.

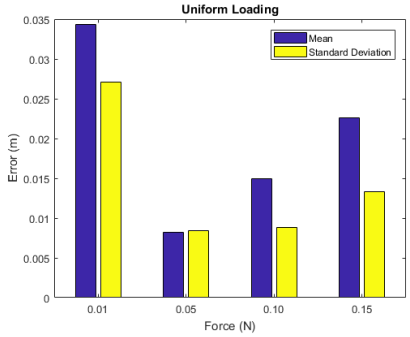

Fig. 8: Summary of mean error and standard deviation of the NROM analysis for the test cases

Overall, the results are promising as the NROM equations are able to predict the deformation of the wing plate for case 1 load cases with a minimum computational complexity and reasonable accuracy since the percentage of error relative to the span of the wing plate is approximately 4%. It is shown that the combination of uniform load cases and twist load cases based NROMs equations are able to predict the deformation of the wing plate subjected to uniform loadings, effectively with minimal error and complexity.

3.1.2. NROM (Case-1, Case-2) for Case-2

Figure 9 presents the summary of mean error and standard deviation of the NROM analysis for the test cases. Based on Figure 9, the maximum mean error was found to be at the test-case with the highest magnitude of force. However, the mean error was found to be of approximately 0.04 rad with a standard deviation of approximately 0.02 rad. However, for the other test-cases, the mean error and the standard deviation of the error is relatively lower in comparison to the test-case with the highest magnitude of force. At extremely high deflections, the error of the NROM analysis increases, this is due to limitations of the equation to which the additional input of mode, test cases and increment in the order of the equation are possible solutions that can be opted to increase the accuracy of the analysis for higher deflection ranges.

Overall, the results are promising as the NROM equations are able to predict the deformation of the wing plate for case 2 load cases with a minimum computational complexity and reasonable accuracy since the percentage of error relative to the rotation of the wing plate when loaded the highest magnitude of force test-case is approximately 6%. It is shown that the combination of uniform load cases and twist load cases based upon NROMs equations are able to predict the deformation of the wing plate subjected to twist loadings, effectively with minimal error and complexity.

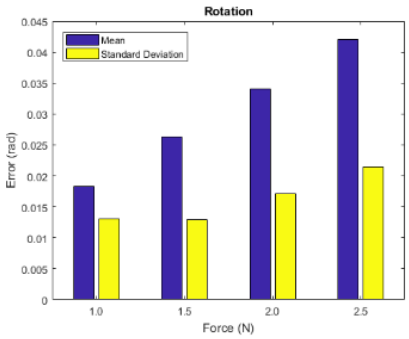

Fig. 9: Summary of mean error and standard deviation of the NROM analysis for the test cases

3.1.3. NROM (Case-1, Case-2) for Case-3

Figure 10 presents the summary of mean error and standard deviation of the NROM analysis for the test cases. Based on Figure 10, the maximum mean error was found to be at the test-case with the lowest magnitude of force for the leading edge and trailing edge deflections. As for the rotation of the wing, the highest mean error was found to be at second test-case which constitutes the second lowest magnitude of force.

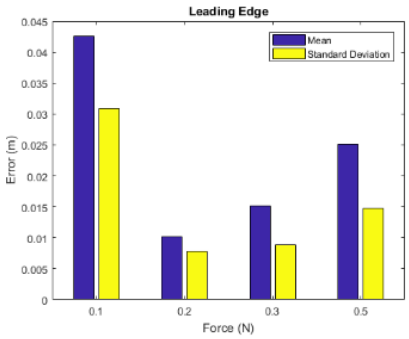

(a) Leading Edge

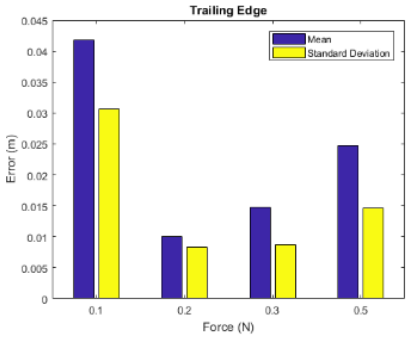

(b) Trailing Edge

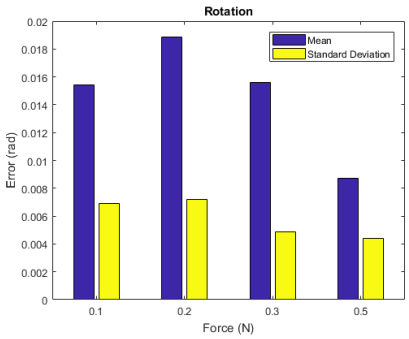

(c) Rotation

Fig. 10: Summary of mean error and standard deviation of the NROM analysis for the test cases

For the leading edge and trailing edge deformations, the maximum error is approximately 4.5 cm. The error is expected due to the nature of the NROM equation which is centred on the nonlinear properties of the wing plate model. Hence, the percentage of error

relative to the span of the wing plate is approximately 5.6%. Moreover, for the rotation of the wing plate model, the maximum mean error is approximately 0.018 rad. However, it was seen the test-case with the highest magnitude of force loading has the lowest error. Although the magnitude of error is relatively small, the percentage of error calculated relative to the maximum rotation of the wing plate at the test-case loading was found to be at 17.7%. Nonetheless, the percentage of error can be dismissed as the deformation of the wing plate itself is very small.

Overall, the results are promising as the NROM equations are able to predict the deformation of the wing plate for case 2 load cases with a minimum computational complexity and reasonable accuracy. It has been shown that the combination of uniform load cases and twist load cases based NROMs equations are able to predict the deformation of the wing plate subjected to leading edge loadings, effectively with minimal error and complexity.

3.2. Investigation of NROM produced with Case-3 test cases to predict deformation due to Case-1, Case-2 and Case-3 loading

NROM equations of Case 2 load cases are summarized in Table 3.

Table 3: NROM equations

$\boldsymbol{F_{B1}} = 153\ P_{B1} + (1.54 \times 10^{3})\ P_{B1}^{2} + (6.01 \times 10^{3})\ P_{B1}^{3}$
$\boldsymbol{F_{T1}} = 146369\ P_{T1} + (9.78 \times 10^{8})\ P_{T1}^{2} + (2.33 \times 10^{12})\ P_{T1}^{3}$

3.2.1. NROM (Case-3) for Case-1

Figure 11 presents the summary of mean error and standard deviation of the NROM analysis for the test cases. Based on Figure 11, the maximum mean error was found at the test-case with the lowest magnitude force. The maximum mean error is approximately 3.5 cm. The error is mainly contributed due to the constriction of the NROM equation which is developed based on the nonlinear properties of the wing plate model. The test-case is shown to have linear properties as shown in Figure 3. Hence, the NROM equation isn't able to characterize the profile of the wing plate model due to its excessive linear properties. The mean errors of other test-cases are found to be relatively lower than the maximum mean error.

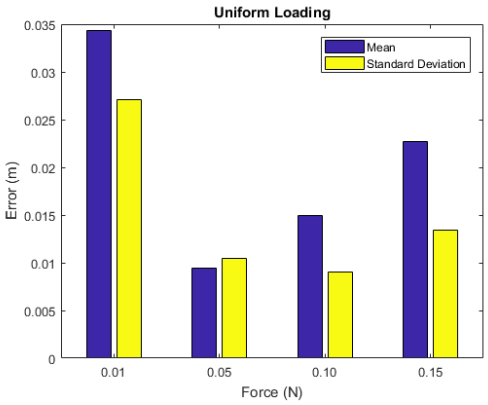

Fig. 11: Summary of mean error and standard deviation of the NROM analysis for the test cases

Overall, the NROM equations were able to predict the deformation of the wing plate due to uniform loading with minimal computational time and reasonable accuracy since the percentage of error relative to the wingspan of the wing plate model is of 4.3%.

3.2.2. NROM (Case-3) for Case-2

Figure 12 shows the summary of mean error and standard deviation of the NROM analysis for the test cases. Based on Figure 12, the maximum mean error is found at the test-case with the highest magnitude of loading force. The maximum mean error is 0.6 rad. The other test-case also show very high error hence showcasing the failure of the NROM equations to characterize the rotation of the wing model. The NROM equations developed were from test-cases used for Case 3 loadings hence the rotational movement of the wing plate model is minimal in comparison to the rotational movement of the wing plate model subjected to Case 2 loadings. Hence, the NROM equations developed aren't characterized with such high rotational movement resulting in such high error.

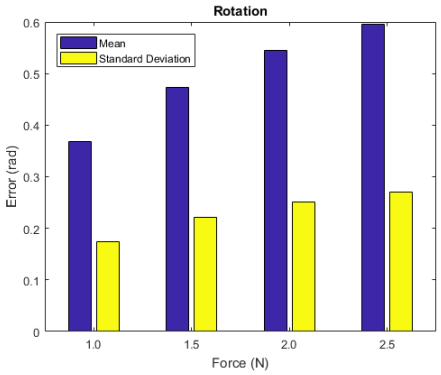

Fig. 12: Summary of mean error and standard deviation of the NROM analysis for the test cases

Overall, the NROM equations from Case 3 test-cases aren't able to predict the deformation of the wing plate model when subjected to Case 2 loadings.

3.2.3. NROM (Case-3) for Case-3

Figure 13 presents the summary of mean error and standard deviation of the NROM analysis for the test cases. Based on Figure 13, the maximum error for the trailing edge and leading edge is at the test-case with the lowest magnitude of force. The mean error for the test-case is approximately 3.5 cm. The resulting high error is again due to the limitations of the NROM equations to characterize the linear properties of the wing plate model. However, the percentage of error relative to the wingspan of the wing plate model for the maximum mean error is 4.3% hence highlighting the reliability of the NROM equations. As for the rotation of the wing plate model, the highest error was found at the test-case with the highest magnitude of force with a mean error of approximately 0.008 rad. The analysis can be considered as accurate since the error is very small but however due to the magnitude of the rotation of the wing plate being small the error is portrayed to be bigger than what it is.

Overall, the NROM equations developed from Case 3 loading test-cases were able to predict the deformation of the wing plate model with minimal computational time and significant accuracy as per discussed above.

3.3. Investigation of NROM produced with all load cases to predict deformation due to Case-1, Case-2 and Case-3 loading

The NROM equations based on Case 1, Case 2 and Case 3 load cases are summarized in Table 4.

Table 4: NROM equations

$\boldsymbol{F_{B1}} = 153\ P_{B1} + (1.53 \times 10^{3})\ P_{B1}^{2} + (5.93 \times 10^{3})\ P_{B1}^{3}$
$\boldsymbol{F_{T1}} = 146369\ P_{T1} + (4.85 \times 10^{7})\ P_{T1}^{2} + (6.65 \times 10^{9})\ P_{T1}^{3}$

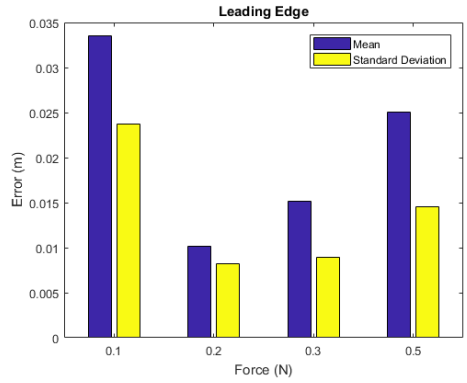

(a) Leading Edge

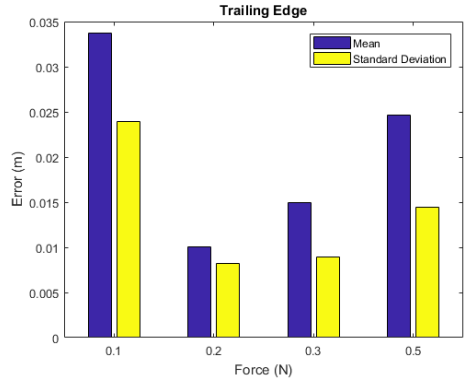

(b) Trailing Edge

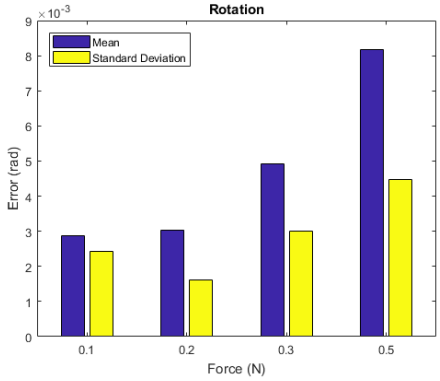

(c) Rotation

Fig. 13: Summary of mean error and standard deviation of the NROM analysis for the test cases

3.3.1. NROM (Case-1, Case-2, Case-3) for Case 1

Figure 14 shows the results of the NROM developed based on the three cases defined to predict the deformations of Case 1 test-cases. The results show very good agreement with the conventional nonlinear analysis as the maximum error is approximately 3.5 cm.

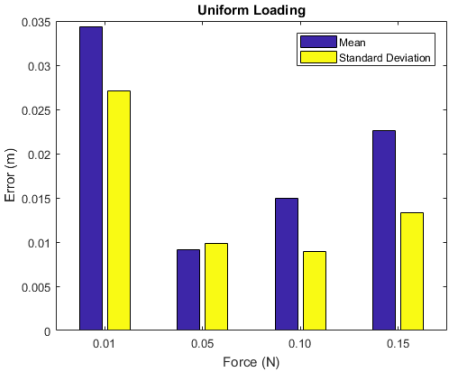

Fig. 14: Summary of mean error and standard deviation of the NROM analysis for the test cases for uniform loading

The maximum error occurs at the test-case with the lowest magnitude of force. The error is expected to be large at the test-case due to the limitations of the NROM equation to predict linear deformations which have been characterized by the test-case. Nevertheless, the NROM is able to successfully predict the deformation of the wing plate mode with minimal computational time and significant accuracy since the percentage of error relative to the wingspan of the wing plate model is approximately 4.3%.

3.3.2. NROM (Case-1, Case-2, Case-3) for Case-2

Figure 15 shows the results of the NROM developed based on the three cases defined to predict the deformations of Case 2 test-cases. Based on Figure 15, the maximum error of the analysis is found at the test-case with the highest magnitude of force loading. The maximum mean error is found to be approximately 0.04 rad. The trend shows the increment of loading causes the error of the analysis to increase. This shows the need for more twist mode inputs to cater for the rotational characteristics in the NROM equations.

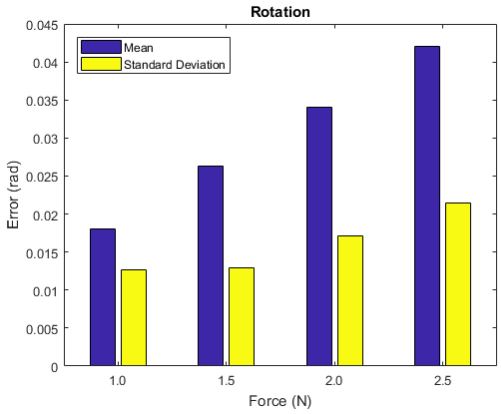

Fig. 15: Summary of mean error and standard deviation of the NROM analysis for the test cases for uniform loading

Overall, the NROM is able to predict the nonlinear deformations of the wing plate for the load cases defined in Case 2 with minimal computational time and significant accuracy as the percentage of error relative to the maximum rotation of the wing plate model is found to be 5%.

3.3.3. NROM (Case-1, Case-2, Case-3) for Case 3

Figure 16 shows the results of the NROM developed based on the three cases defined to predict the deformations of Case 2 test-cases. Based on Figure 16, the maximum error was found to occur at test-case with the lowest magnitude force for the leading edge and trailing edge. The maximum error for the leading edge and trailing edge deformation is approximately 3.8 cm. The error is mainly due to the inability of the NROM to predict linear deformations since the NROM equations are developed with nonlinear characteristics. While the maximum error for the rotational deformation of the wing was found to be of approximately 0.018 rad. The error is considered to be small due to the minimum rotation of the wing plate model at the test-case. The NROM produced can be categorized to be a success as it was able to predict the nonlinear deformation of the wing plate with significant accuracy and lower complexity since the percentage of error relative to the wingspan of the wing plate model is found to be of 4.8%. The percentage of error for the rotation of the wing plate isn't considered as the rotation of the wing plate is small will only amplify the error to be a large number whilst the error is not very significant.

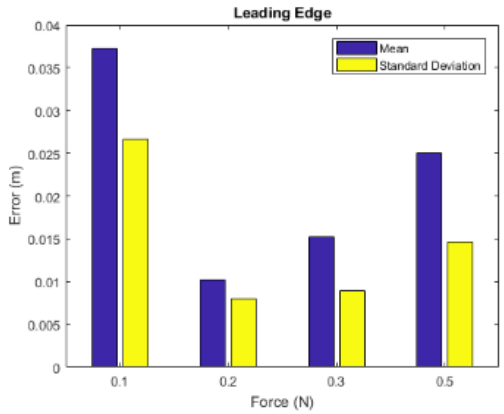

(a) Leading Edge

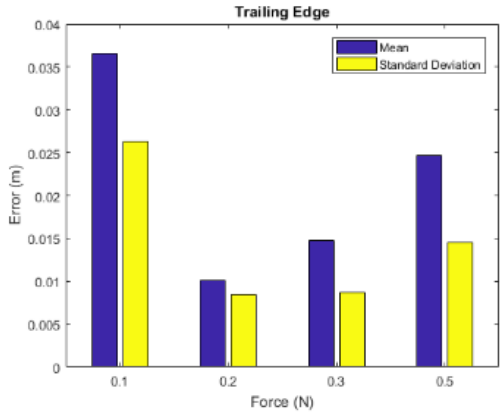

(b) Trailing Edge

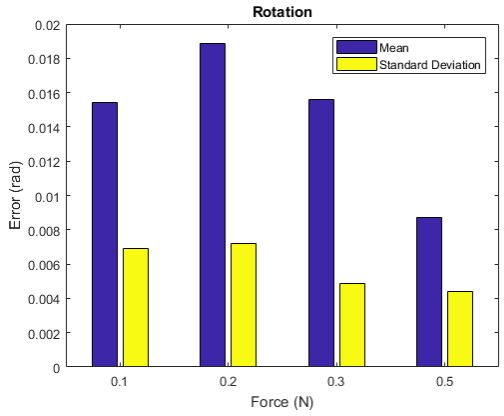

(c) Rotation

Fig. 16: Summary of mean error and standard deviation of the NROM analysis for the test cases

4. Conclusion

CMFE approach based NROMs have been developed using the prescribed case types and respective test cases to predict the nonlinear behaviour of the wing plate model. The results of the NROMs developed are promising with significant accuracy being achieved. In addition, the complexity present in the conventional nonlinear static analysis is reduced to improve the computational time of the analysis. The NROMs provide an option for the user to tailor the accuracy accordingly by increasing the normal mode inputs or the load case inputs sacrificing some degree of computational efficiency. Most of the NROMs developed are significantly accurate with exception to the NROM based on the Case 3 loadings, which has an extremely high error for the rotational deformation of the wing plate. When comparing all NROMs produced, the NROM based on all the load cases has the lowest maximum error count. The NROM produced is able to predict the nonlinear deformations with good accuracy while at the same time conveniently reducing the complexity when compared to conventional complex nonlinear analysis. The NROMs are feasible to be used for more convenient nonlinear static analysis of HAR wing plates. Although in this study the approach is implemented on a simple wing plate, the same approach and technique can be implemented on a real size aircraft wing. The research is to be continued with experimental validation and with the motive of optimizing the NROMs for more accurate answers without much sacrifice to the computational time.

Acknowledgement

The authors acknowledge the financial support from Ministry of Education (MOE) Malaysia for this study through the Fundamental Research Grant Scheme (FRGS/1/2015/TK09/UPM/02/2) with Project Code: 03-01-15-1625FR.

References

[1] Ahmad K, Wuzhigang W & Rahman H (2013), Aeroelastic analysis of high aspect ratio wing in subsonic flow. 10th International Bhurban Conference on Applied Sciences & Technology

[2] Kermode AC, Barnard RH & Philpott DR (2012). *Mechanics of flight*. Harlow: Pearson.

[3] Barrett P (2016), Understanding geometric nonlinearities. Retrieved from https://caeai.com/blog/understanding-geometric-nonlinearities

[4] Charmbalis G & Cooper JE (2013). Vibration testing of aeroelastic structures containing geometric stiffness nonlinearities. AIAA / ASME / ASCE / AHS / ASC Structures, Structural Dynamics, and Materials Conference

[5] Dowell EH, Edwards J & Strganac T (2003), Nonlinear aeroelasticity. *Journal of Aircraft* 40(5), 857-874

[6] Harmin MY & Cooper JE (2011), Aeroelastic behaviour of a wing including metric nonlinearities. *The Aeronautical Journal* 115(1174), 767-777

[7] Noll TE, Brown JM, Perez-Davis ME, Ishmael SD, Tiffany GC & Gaier M (2004), Investigation of the Helios Prototype Aircraft Mishap. National Aeronautics and Space Administration

[8] Dunbar B (2007.), Helios crash probed. Retrieved from https://www.nasa.gov/missions/research/helios.html

[9] Patil MJ, Hodges DH & Cesnik CE (2001), Nonlinear aeroelasticity and flight dynamics of high-altitude long-endurance aircraft. *Journal of Aircraft* 38(1), 88-94

[10] Cesnik CES, Palacios R & Reichenbach EY (2014), Reexamined structural design procedures for very flexible aircraft. *Journal of Aircraft* 51(5), 1580-1591

[11] McEwan MI, Wright JR, Cooper JE & Leung AYT (2011), A finite element/modal technique for nonlinear plate and stiffened panel response prediction. AIAA/ASME/ASCE/AHS/ASC Structures, Structural Dynamics and Materials Conference and Exhibit

[12] Castellani M, Lemmens Y & Cooper JE (2015), Parametric reduced-order model approach for simulation and optimization of aeroelastic systems with structural.nonlinearities. *Proceedings of the Institution of Mechanical Engineers, Part G: Journal of Aerospace Engineering* 230(8), 1359-1370